https://doi.org/10.5194/egusphere-2025-753
Preprint. Discussion started: 10 April 2025

DRIVE v1.0: A data-driven framework to estimate road transport emissions and temporal profiles

Daniel Kühbacher[1], Jia Chen[1], Patrick Aigner[1], Mario Ilic[3], Ingrid Super[2], and Hugo Denier van der Gon[2]

[1]Professorship of Environmental Sensing and Modeling, Technical University of Munich
[2]Department of Climate, Air and Sustainability, TNO, Utrecht, Netherlands
[3]Chair of Traffic Engineering and Control, Technical University of Munich

Correspondence: Daniel Kühbacher (daniel.kuehbacher@tum.de) and Jia Chen (jia.chen@tum.de)

Abstract. Traffic in urban areas is an important source of greenhouse gas (GHG) and air pollutant emissions. Estimating traffic-related emissions is therefore a key component in compiling a city emission inventory. Inventories are fundamental for understanding, monitoring, managing, and mitigating local pollutant emissions.

We present DRIVE v1.0, a data-driven framework to calculate road transport emissions based on a multi-modal macroscopic traffic model, vehicle class-specific traffic counting data from more than a hundred counting stations, and HBEFA emission factors. DRIVE introduces a novel approach for estimating traffic emissions with vehicle-specific temporal profiles in hourly resolution. In addition, we use traffic counting data to estimate the uncertainty of traffic activity and the resulting emission estimates at different temporal aggregation levels and with road link resolution. The framework was applied to the City of Munich, covering an area of 311 km^2 and accounting for GHGs (CO_2, CH_4) and air pollutants (PM, CO, NO_x). It captures irregular events such as COVID lockdowns and holiday periods well and is suitable for use in near real-time applications. Emission estimates for 2019-2022 are presented and differences in city totals and spatial distribution compared to the official municipal reported and national and European downscaled inventories are examined.

1 Introduction

Urban areas are centers of human activity that contribute to high greenhouse gas (GHG) emissions and poor air quality. As the global population becomes increasingly urbanized, cities face the dual challenge of supporting economic growth and development while mitigating environmental impacts. 75 % of the world's primary energy, mainly in the form of fossil fuels, is consumed in cities, resulting in 70 % of global CO_2 emissions (IEA, 2024). A substantial portion of urban greenhouse gases and air pollutants are associated with transportation, mainly from road vehicles (Chapman, 2007; Edenhofer et al., 2014; Crippa et al., 2021). These emissions not only exacerbate climate change but also pose a severe health risk to the urban population through exposure to poor air quality. The European Environment Agency (EEA) attributes 307,000 premature deaths to chronic exposure to particulate matter and 40,400 deaths to nitrogen dioxide exposure in Europe (EEA, 2022).

Understanding the sources, magnitude, and trends of transport emissions is crucial for developing effective mitigation strategies. A road transport emission inventory provides a detailed assessment of emissions from different transport modes, enabling

https://doi.org/10.5194/egusphere-2025-753
Preprint. Discussion started: 10 April 2025

the identification of key sources and the evaluation of mitigation measures (Ting Wei et al., 2021; Arioli et al., 2020). In the German Climate Action Plan, a mid-term goal has been set to reduce GHG emissions from the transport sector by 40-42 % by 2030 compared to 1990 levels (BMUB, 2016). The City of Munich aims to reduce traffic-related GHG emissions by 58 % by 2035 compared to 2018 levels (Timpe et al., 2021). Moreover, the World Health Organization (WHO) has lowered the annual threshold values for NO_2 from 40 $\mu g/m^3$ to 10 $\mu g/m^3$ and for PM_{10} from 20 $\mu g/m^3$ to 15 $\mu g/m^3$ in its current air quality guidelines (WHO, 2021). Meeting these ambitious goals demands accurate emission estimates as an essential resource for policymakers, urban planners, and environmental scientists.

High spatial and temporal resolution becomes essential when inventories are used alongside observations and atmospheric transport models. Methodologies exist to disaggregate nationally reported emissions on spatial and temporal scales using proxy information (e.g., population count, road density). Popular examples of inventories following that top-down approach utilizing different spatial proxy maps are ODIAC (Oda and Maksyutov, 2011; Oda et al., 2018), and CAMS-REG-v4 (Kuenen et al., 2022). The German Federal Environmental Agency (UBA) also provides gridded emissions for Germany using national proxy data or spatially disaggregated activity data (Schneider et al., 2016). However, these top-down emission distribution approaches are highly uncertain on a cell scale (Super et al., 2020) and might instead reflect the emission proxy more than the actual emissions (Hutchins et al., 2017).

For the transport sector, data from traffic counting stations, traffic models, and driving patterns are used to accurately capture local activity. Methods based on this granular activity information are generally called bottom-up methods. The activity data can be combined with a range of emission models such as HBEFA (Handbook Emission Factors for Road Transport) (Notter et al., 2019), COPERT (Computer Programme for the Calculation of Emissions from Road Transport) (Ntziachristos and Samaras, 2024) or PHEM (Passenger Car and Heavy Duty Emission Model) (Hausberger, 2003) to enable bottom-up emission estimation. They can be classified based on how they incorporate traffic behavior, though more complex emission models do not necessarily perform systematically better (Smit et al., 2010). HBEFA and COPERT use average speeds or distinct traffic situations and road types to consider average traffic behavior. PHEM takes a more detailed approach by incorporating second-by-second vehicle operating data to reflect instantaneous driving conditions.

Various frameworks also implement these emission models to estimate road transport emissions at high spatiotemporal resolution. Each is designed for distinct target areas, user groups, and applications. VEIN implements COPERT and other methods focusing on developing countries (Ibarra-Espinosa et al., 2018). HERMESv3 includes a bottom-up module with a coupled macroscopic traffic and emission modeling system targeting the Barcelona metropolitan area (Rodriguez-Rey et al., 2021; Guevara et al., 2021). CARS (Baek et al., 2022) and Yeti (Chan et al., 2023) are both Python-based and were implemented for Seoul (South Korea) and Berlin (Germany), respectively. The traffic models these frameworks use typically provide road-specific, time-aggregated information for a representative weekday or peak hours. This information is either used to distribute aggregated emission estimates or temporally extrapolated with generalized traffic activity profiles. However, they do not leverage the full potential of local activity time series for temporal extrapolation or uncertainty assessment. A more activity-data-intensive approach is to use floating car data (FCD; GPS information of individual vehicles) or information from intelligent traffic monitoring systems (ITMS) (Jiang et al., 2021; Wen et al., 2020; Wu et al., 2020; Yang et al., 2019; Gately et al., 2017). This data

https://doi.org/10.5194/egusphere-2025-753
Preprint. Discussion started: 10 April 2025

provides exact speed and congestion information with high spatiotemporal resolution. Nevertheless, data protection concerns and substantial costs by commercial data providers widely restrict the use and availability of these information sources. In contrast, conventional traffic counting data (e.g., from induction loop meters) is widely available in most cities, highlighting the potential for more extensive use of these datasets for local, data-driven emissions modeling.

With this work, we present a road transport emission inventory framework (DRIVE v1.0; Data-driven Road-Transport Inventory for Vehicle Emissions Version 1.0), written in Python, that combines a comprehensive macroscopic traffic model, vehicle-specific traffic counting data, and HBEFA emission factors. Our novelty is the extensive use of counting data from more than 100 individual traffic detectors across different road types within our area of interest. First, the local counting data is used to extrapolate the traffic model over time. Next, we introduce a novel method for data-based and time-resolved calculation of the vehicle share. The vehicle class-specific temporal scaling of traffic activity also enables a precise prediction of traffic conditions and the use of HBEFA emission factors at the most detailed level. Finally, we assess model uncertainties based on the counting data. With the possibility of accessing local data in real-time, our method is suitable for near-real-time applications, such as the assessment of air quality or greenhouse gas mitigation measures.

The framework is implemented for the City of Munich, representing Munich's first spatially and temporally explicit bottom-up traffic inventory, covering all road-based vehicle categories. It accounts for GHG emissions like carbon dioxide (fossil-fuel: $CO_{2,ff}$, fossil- and bio-fuel: $CO_{2,ff+bf}$), methane (CH_4), and co-emitted species such as carbon monoxide (CO), nitrous oxides (NO_x) and particulate matter (PM_{10}). Our data-driven approach effectively captures special events such as the COVID-19 pandemic, vacation periods, and Christmas. We compare our estimates to city-reported figures and national and European datasets available for the Munich region. The resulting emission- and uncertainty estimates and temporal profiles are invaluable for the timely evaluation of mitigation measures and atmospheric modeling of greenhouse gases and air pollutants.

2 Methodology

The most relevant traffic activity variables for emission modeling are the traffic flow, vehicle-specific information (type, age, category, size), speed, road network, and fuel used (Pinto et al., 2020). Data availability remains the most significant challenge and sets inherent limits to implementing traffic emission inventories (Arioli et al., 2020). The availability of activity data determines the selection of the emission model and the associated emission factors. Our framework exploits traffic data available in our target city, Munich. Subsequently, HBEFA 4.2 emission factors are applied, as they are also utilized and regularly updated by Germany's Federal Environment Agency. These factors incorporate national statistical data on the vehicle fleet, including age, size, fuel type, and EURO emission class parameters. Figure 1a shows an overview of the proposed methodology. Static traffic information derived from a traffic model is combined with dynamic traffic information from traffic counting stations to estimate the hourly traffic volume and condition for every road segment in the model.

https://doi.org/10.5194/egusphere-2025-753
Preprint. Discussion started: 10 April 2025

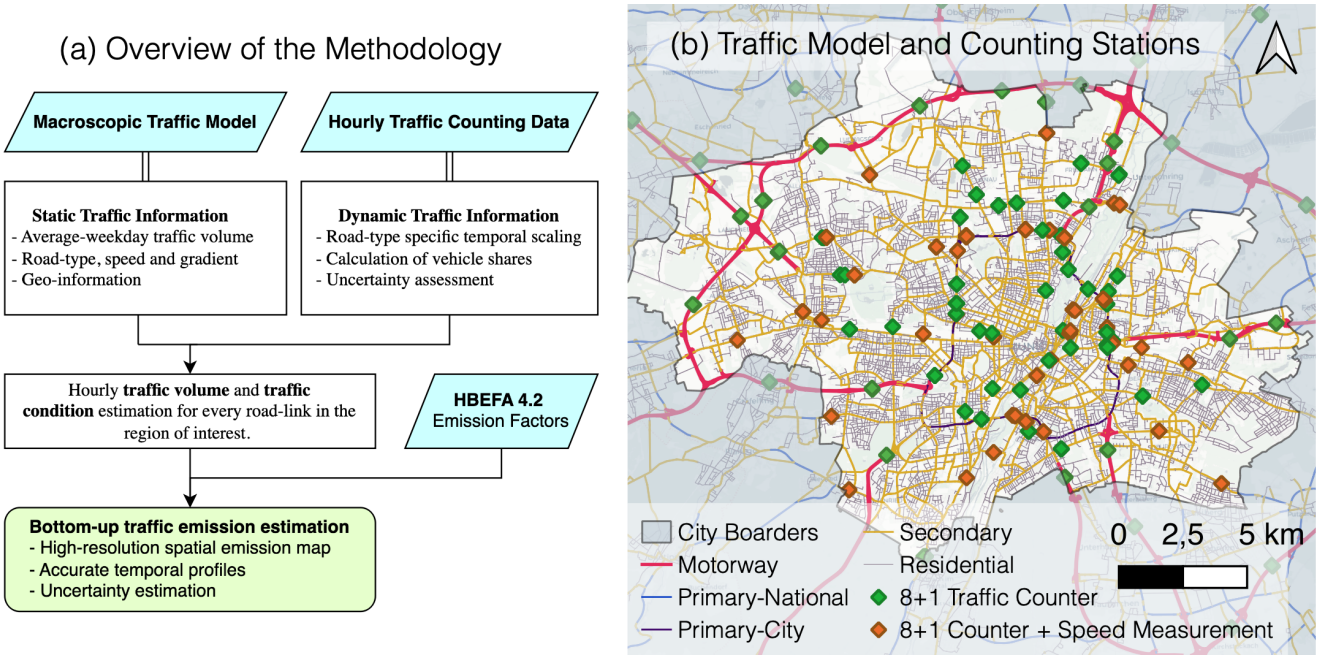

Figure 1. Overview of the methodology and data applied in the present study. (a) depicts how static and dynamic traffic activity data is used to calculate the hourly traffic volume and condition. Subsequently, HBEFA emission factors are applied to calculate emissions. (b) provides an overview of the study area and indicates the locations of traffic counting stations in the region of interest. Each traffic counter shown provides vehicle-specific counts, and 43 stations also provide average speed measurements. 116 individual counting stations are available in our area of interest.

2.1 Traffic Activity Data

2.1.1 Traffic Model

Many medium-sized to large cities maintain macroscopic traffic models for infrastructure planning, simulating traffic volumes, or analyzing travel demand scenarios. They are calibrated with observations like traffic counts, speed measurements, and data from mobility behavior surveys. The City of Munich maintains a macroscopic traffic demand model for the city area and surrounding municipalities based on PTV's (Planung Transport Verkehr GmbH) software VISUM. The year of analysis is 2019. It represents the average annual norm-weekday (Tuesday-Thursday outside the holiday season) traffic volume $q_{i,vc}^{model}$ for passenger cars (PC), light commercial vehicles (LCV), heavy goods vehicles (HGV), and public transport. The model data was exported for our region of interest providing the traffic volume $q_{i,vc}^{model}$ [veh/day] of the aforementioned vehicle classes, the speed limit v_i [km/h], road type r_i, road gradient s_i [%], hourly road capacity C_i [veh/h] and geoinformation for each road link i of the model.

https://doi.org/10.5194/egusphere-2025-753
Preprint. Discussion started: 10 April 2025

2.1.2 Traffic Counting Data

Camera-based and induction loop traffic counters are frequently used for monitoring and management. We utilize hourly traffic counting data to scale the average weekday traffic volumes from the traffic model to each day within the study period. In addition, the data is used to create diurnal traffic patterns that assign daily traffic volumes to specific hours of the day. Details on the temporal scaling are presented in section 2.2.

In total, 116 traffic counters are available in our region of interest. The city administration maintains 82 stations within the urban region, while the BASt (Bundesagentur für Straßenbau, eng.: Federal Road Agency) provides counting data from 34 locations on national motorways and federal primary roads. Both data sources categorize the counts into eight vehicle classes (passenger cars, passenger cars with trailers, light commercial vehicles, heavy trucks, heavy trucks with trailers, semi-trailer trucks, motorcycles, and buses) and one category for unclassified vehicles. Some stations also provide the average speed of vehicles, but this data is not used in the model as it is unreliable. In figure 1b, the locations of the counting stations are superimposed on Munich's road network. Some stations were excluded because they lacked data for the study period or were densely clustered near specific locations, such as the trade fair area or Allianz Arena (soccer stadium).

2.1.3 Data Preprocessing

Manual data curation and automatic preprocessing are required to make the traffic counting data compatible with the traffic model and to pass on counting data to the processing modules provided by the framework. The first step is to convert traffic count information from different sources to a standard data model (see Appendix B1). For this, the location of the traffic detectors must also be allocated to the respective road link in the traffic model on which the data is observed. It enables the model data to be combined with counting data and the counting data to be supplemented with road link details. If multiple detectors are located on the same road link, the counting data has to be aggregated subsequently. Additionally, the 8+1 vehicle classification from the traffic counting data needs to be aggregated into vehicle classes that are compatible with the HBEFA classification (see Appendix B2).

A modified z-score (Iglewicz Boris and David C. Hoaglin, 1993) is applied to the daily count value for outlier detection. The counting data is grouped by vehicle class, day, and road type, and a z-score threshold of ± 3.5 is applied. Additionally, we compare the total daily count and the sum of all hourly counts. If these values do not match, the error is usually due to communication problems between the detectors and the traffic management center (Lu et al., 2008). We defined an error margin of $\pm 5\%$ for the sum of the hourly counts compared to the daily count, outside of which the data rows are removed.

Two additional attributes, *"complete"* and *"valid"*, were added to the counting data to filter out time series that are not suitable for the temporal extrapolation of the traffic model (see section 2.2). *"Complete"* time series were empirically defined as series that cover more than 80 % of all days in the time period of interest. The *"valid"* property indicates how well the counted traffic volume matches the traffic volume provided by the traffic model. A bad fit is related to improper model calibration, hardware faults of the traffic detectors, wrong assignment of the counting station to the traffic model, or inconsistent detector identifiers. The Scalable Quality Value (SQV) (Friedrich et al., 2019) is used to assess the fit between counting data and the traffic model.

https://doi.org/10.5194/egusphere-2025-753
Preprint. Discussion started: 10 April 2025

It is a measure between 0 (no fit) and 1 (perfect fit). From the counting data, we calculate the annual average weekday traffic volume for 2019 $q_{i,vc}^{count,ref}$ for each road link with an assigned counting station. This value is representative of the one in the traffic model, allowing for direct comparison. An SQV-threshold of 0.6 covers > 90 % of the stations, which were subsequently flagged as *"valid"*.

2.2 Temporal Scaling

This section describes our methodology for extrapolating traffic model information using the preprocessed counting data. First, three different road categories r_i are defined for scaling: Motorway, primary city, and distributor/secondary roads. Residential, local, and distributor roads (i.e., minor roads) are scaled using the same factor because significant differences in activity were not observed, and no detectors are available on lower-level roads. Next, we define three different day types d: Weekday (Monday to Friday), Saturday, and Sunday/Holiday. They all show individual activity behavior. Finally, we incorporate the HBEFA vehicle class categorization, distinguishing between passenger cars (PC), light commercial vehicles (LCV), heavy goods vehicles (HGV), motorcycles (MOT), and coaches (BUS).

Equation 1 shows the calculation of the hourly traffic volume and is applied to each road link in the traffic model. The $q_{i,vc}^{model}$ is scaled to any day in the time period of interest using the annual cycle of the present road type α_r (details in subsection 2.2.1). We assume that the activity on roads of the same type scales identically. The total traffic volume is then split among all vehicle classes using the road-type dependent vehicle share $\delta_{vc,r}$ (details in subsection 2.2.2). Additional correction factors $\kappa_{i,vc}$ were computed to incorporate spatial differences in vehicle shares (e.g., arterial motorways have a lower HGV share than the ring motorway). Vehicle and day-type individual diurnal cycles $\beta_{vc,d}$ (details in subsection 2.2.3) are applied to obtain an hourly traffic volume $q_{i,vc}$.

$$q_{i,vc} = q_{i,vc}^{model} \cdot \alpha_r \cdot \beta_{vc,d} \cdot \delta_{vc,r} \cdot \kappa_{i,vc} \tag{1}$$

2.2.1 Annual Cycles

For scaling, the counting time series are normalized to the reference time period that the traffic model represents. In our implementation, the model represents the average norm weekday of 2019. Therefore, each counting time series was normalized by the average norm-weekday count of 2019 $q_{i,vc}^{count,ref}$. The time series were then grouped by road type, and the median of the normalized daily traffic volume of all *"valid"* and *"complete"* time series was calculated. It results in three separate annual cycles α_r for the road type "Motorway-National", "Trunk Road/ Primary-City", and "Distributor/Secondary" which also covers lower-level road types. Missing values were imputed using an average scaling factor from normalized counts of the identical day type in the adjacent months.

Figure 2 shows the annual "Distributor/Secondary" streets cycle from 2019 to 2022. A strong periodic drop in traffic activity can be observed on weekends. The traffic activity also captures special events like vacation and holiday times or the lockdown influence of the COVID-19 pandemic.

https://doi.org/10.5194/egusphere-2025-753
Preprint. Discussion started: 10 April 2025

Figure 2. (a) Daily scaling factors derived from traffic counts for the years 2019 to 2022. The plot shows the normalized median count of all counting stations assigned to road links of the type "Distributor/Secondary". Each counting station's time series was normalized by its average 2019 norm-weekday count. (b) A weekly cycle in July 2019 displays the weekly pattern, showing consistent traffic from Monday to Friday and decreased activity on Saturday and Sunday.

2.2.2 Vehicle Shares

We calculate the daily vehicle shares on different road types based on vehicle-specific counting time series and correct it with average weekday vehicle shares from the traffic model. A set of *valid* and *complete* time series were selected and grouped by vehicle class and road type. Daily median traffic volumes are computed for each group (e.g., median passenger car count of all counting stations located on a motorway). To acquire the vehicle share $\delta_{vc,r}$ for a specific road type, we divide the median count of individual vehicle types by the sum count. Figure 3 depicts the vehicle share time series on "Distributor/Secondary" streets in 2019. We use additional correction factors as the vehicle shares on roads of the same road type are not spatially homogeneous. Our traffic model provides vehicle class-specific traffic volumes for HGV and LCV. They are used to infer average weekday shares $\delta^{model}_{i,HGV}$ and $\delta^{model}_{i,LCV}$ for each road link. We also calculate the average weekday share of the reference year 2019 based on the counting data $\delta^{count,ref}_{HGV,r}$ and $\delta^{count,ref}_{LCV,r}$. The ratios $\kappa_{i,HGV}$ and $\kappa_{i,LCV}$ are used to correct the corresponding vehicle share. To maintain the property that the sum of all shares $\delta_{vc,r}$ equals one after correction, the remaining shares $\delta_{[PC,BUS,MOT],r}$ are corrected with $\kappa_{i,vc}$. It is the ratio between the residual share of all corrected vehicle shares and the uncorrected vehicle shares. Table 1 shows the correction factors and formulas applied.

2.2.3 Diurnal Cycles

The daily cycle $\beta_{vc,d}$ is required to distribute the daily traffic volume to each hour. Diurnal patterns are similar for road and day types but differ for vehicle classes. The hourly traffic counts were normalized by the daily sum count and grouped by day type d and vehicle class vc. For each month, a median cycle was calculated for each category. Figure 4 shows the diurnal cycle of PC on three different day types for 2019. Peaks during rush hours are pronounced in the weekday diurnal cycle. The Saturday

https://doi.org/10.5194/egusphere-2025-753
Preprint. Discussion started: 10 April 2025

Table 1. Formulas to calculate vehicle share correction factors $\kappa_{i,vc}$ based on vehicle shares derived from the traffic model and the traffic counters. These correction factors are used to incorporate spatial differences in vehicle shares.

Vehicle Class	Correction Factor
Heavy goods vehicle (HGV)	$\kappa_{i,HGV} = \delta^{model}_{i,HGV} / \delta^{count,ref}_{HGV,r}$
Light cargo vehicle (LCV)	$\kappa_{i,LCV} = \delta^{model}_{i,LCV} / \delta^{count,ref}_{LCV,r}$
Personal car (PC)	
Coach (BUS)	$\kappa_i = \frac{1-\kappa_{i,HGV} \cdot \delta^{count}_{HGV,r} - \kappa_{i,LCV} \cdot \delta^{count}_{LCV,r}}{1-\delta^{count}_{HGV,r} - \delta^{count}_{LCV,r}}$
Motorcycles (MOT)	

$\kappa_{i,[HGV,LCV]}$ ... Vehicle share correction factor for HGV and LCV for the i-th road link.

κ_i ... Vehicle share correction factor for all remaining vehicle classes for the i-th road link.

$\delta^{model}_{i,[HGV,LCV]}$ ... Average weekday vehicle share of LCV and HGV, derived from the traffic model for the i-th road lin,k.

$\delta^{count,ref}_{[HGV,LCV],r}$ ... Average weekday vehicle share of LCV and HGV, derived from the 2019 counting data on the respective road type.

$\delta^{count}_{[HGV,LCV],r}$ ... Vehicle share of LCV and HGV derived from daily counting data on the respective road type.

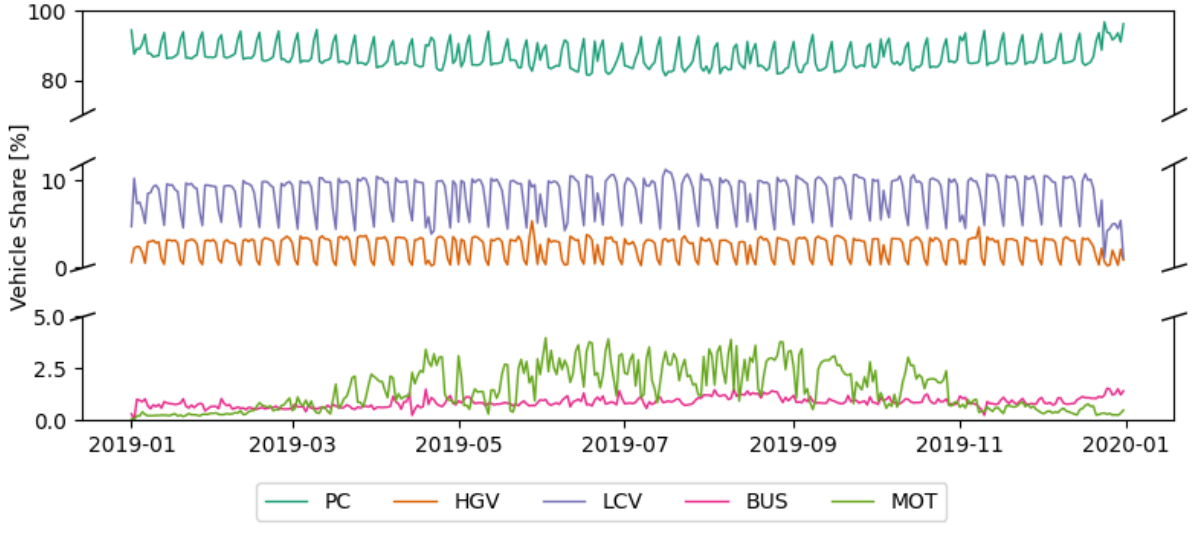

Figure 3. Vehicle share of all vehicle classes on distributor streets in 2019. PCs have the highest share of the total traffic, followed by LCVs, HGVs, MOTs, and Buses. A weekly pattern is observed for PC, LCV, and HGV, with an increase in the PC share and a decrease in the LCV and HGV share over the weekend. MOT shows an annual cycle, a trend that fits with the fact that motorbikes are more likely to be on the road on warm, sunny days. The share of BUS and MOT in total traffic is in the lower single-digit percentage range.

and Sunday/Holiday cycles have a similar shape with a shift in time. Diurnal cycles for other vehicle classes can be found in appendix C1.

https://doi.org/10.5194/egusphere-2025-753
Preprint. Discussion started: 10 April 2025

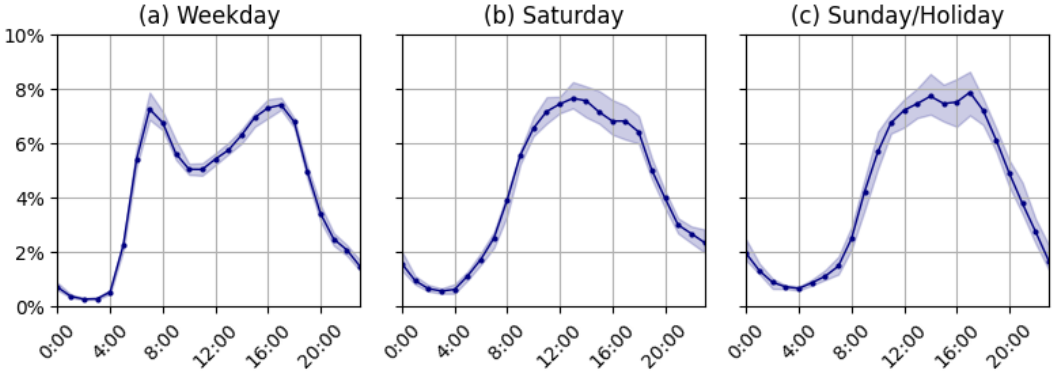

Figure 4. 2019 diurnal cycles of three different day types for PC traffic. The blue line represents the average cycle for all months of the year, while the blue-shaded area indicates the range within which the cycles of individual months fall. Individual cycles are computed for each vehicle class and month of the year.

2.3 Emission Factor Selection

HBEFA distinguishes 365 different traffic situations by considering the road type, road gradient, speed limit, area type (rural vs. urban), and the level-of-service (los) (Notter et al., 2019). The road type, gradient, and speed limit are static for each road link, and the area type "urban" is used for the whole city area. The los is estimated for each road link using the volume-capacity ratio x_i (equation 2) and dedicated thresholds to distinguish between five classes: Freeflow, Heavy, Saturated, Stop&Go, and Stop&Go2 (gridlock). Hour capacity C_i is an attribute of the traffic model. The vehicle-specific hourly traffic volume $q_{i,vc}$ is the product of the traffic model and the aforementioned temporal scaling factors (equation 1). Furthermore, the traffic volume is scaled to passenger car units (PCU) to account for different vehicle sizes. The scaling factors n_{vc} can be found in appendix B2.

$$x_i = \frac{\sum_{vc} q_{i,vc} \cdot n_{vc}}{C_i} \tag{2}$$

Volume-capacity ratio thresholds to distinguish between los classes cannot be universally applied. It is inevitable to validate and optimize them based on reference values. Schmaus et al. (2023) investigated the distribution of the vehicle kilometers traveled (VKT) among different los classes in Germany based on floating car data. We used this information to adjust the VCR thresholds for different road types until the share of the VKT was within 1% of the reference value. This application-specific procedure is described in more detail in the supplement.

2.4 Hot Vehicle Exhaust Emissions

The vehicle kilometers traveled (VKT) is calculated by multiplying the hourly, vehicle-specific traffic volume $q_{i,vc}$ with the geometric length of the road link L_i. Multiplying the VKT with a parameterized emission factor $EF^{hot}_{p,vc,r,s,v,los}$ results in the

https://doi.org/10.5194/egusphere-2025-753
Preprint. Discussion started: 10 April 2025

hot vehicle exhaust emission $E^{hot}_{i,p,vc}$ (equation 3). The emission factors are available for the average annual fleet composition of the corresponding vehicle class vc and different pollutants p. Further parameters are the road type r_i, road gradient s_i, the maximum allowed speed v_i, and the level of service los.

$$E^{hot}_{i,p,vc} = q_{i,vc} \cdot EF^{hot}_{p,vc,r,s,v,los} \cdot L_i \tag{3}$$

2.5 Cold Start Excess Emissions

A "cold start" is the first minutes following the combustion engine's first start. The cold start period ends when the coolant reaches 343 K (70 °C) for the first time, but no later than five minutes after the initial engine start. (EC-JRC, 2017)

HBEFA provides emission surcharges $EF^{cold}_{p,vc,T}$ in grams per vehicle cold start differentiated by trip duration, length, and ambient temperature for passenger cars and light commercial vehicles. Trucks, buses, and motorcycles are therefore neglected in the following. Statistical averages were chosen for the duration and length of the trips, as this information is not available spatially resolved. A value-binned (-10°C, -5°C, 0°C, 5°C, 10°C, 15°C, 20°C, 25°C) hourly ambient temperature T for Munich was derived from meteorology measurement data available in the city center. The spatially distributed number of the vehicle starts N_{vc} is available in the traffic model utilized in the study and was modulated using vehicle-specific temporal scaling factors for the road type "Distributor/Secondary."

The distance traveled and time taken for the engine to reach nominal temperatures are difficult to determine. So emissions are assigned to all roads except the motorway within a 1.5 km surrounding buffer. This radius represents how far vehicles can travel in the first 90 seconds at 60 km/h. A weighting factor was determined to distribute the emissions in relation to the traffic volume. This factor is calculated for each road link from the quotient of the traffic volume of the link and the sum of all traffic volumes of the links in the buffer zone. We assume a constant spatial distribution of cold start surcharges, as no separate information is available for days other than the average weekday of 2019.

$$E^{cold}_{i,p,vc} = N_{vc} \cdot EF^{cold}_{p,vc,T} \tag{4}$$

3 Results and Discussion

3.1 Annual Activity Data

Our proposed method combines a macroscopic traffic demand model with traffic counting data on different road types to achieve a data-based temporal scaling of traffic activity for emissions calculation. The primary result is an estimate of the vehicle kilometers traveled (VKT) for different vehicle classes and the respective traffic conditions. Figure 5a shows the annual VKT for 2019-2022. A 12,7 % decrease in the yearly VKT is present in 2020, which can be related to significantly reduced traffic activity due to the COVID-19 pandemic (Anke et al., 2021; Creutzig et al.). VKT increased by 1.5 % in 2021 and a further 3.5 % in 2022 compared to the previous year. The distribution of VKT across the different LOS classes has also

https://doi.org/10.5194/egusphere-2025-753
Preprint. Discussion started: 10 April 2025

changed over the years. In 2019, 53 % of the total vehicle kilometers traveled occurred under free-flow traffic conditions, which increased to 59 % in 2020. More kilometers have also been assigned to the traffic condition *Stop&Go* and *Stop&Go 2* in 2019 compared to other years. This indicates that traffic has become more fluid due to lower traffic volume in recent years.

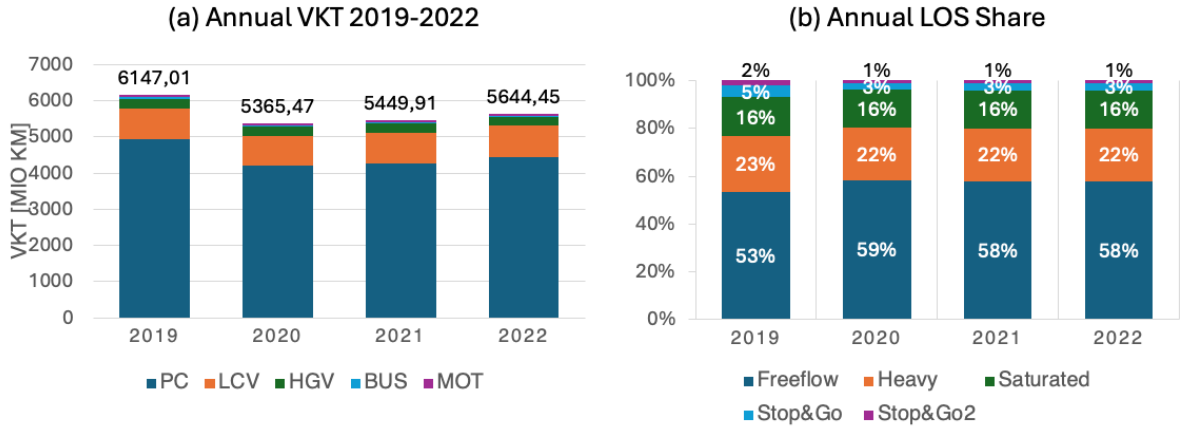

Figure 5. (a) depicts the total annual VKT in Munich for 2019-2022. A strong decrease due to COVID-19 is present in 2020. Since then, traffic activity has been growing but has not reached pre-COVID levels yet. (b) shows the relative distribution of the total VKT to different LOS classes. The reduced traffic in 2020 resulted in more free-flow traffic and fewer kilometers traveled in highly congested conditions. The distribution is similar for 2020-2022.

The City of Munich's Department for Climate and Environmental Protection (RKU) bi-annually estimates the city's greenhouse gases. The most recent numbers are available for 2019 (Referat für Klima und Umweltschutz, 2022). On request, we received a more detailed evaluation, which splits emissions and the corresponding kilometers driven into total traffic and heavy goods traffic.

Their calculation is based on the BISKO Method (Bilanzierungs-Systematik Kommunal, eng.: Municipal Accounting System, IFEU (2019)) and is performed by analyzing the local final energy consumption. The emission factors for subsequent GHG calculation also consider upstream emissions. Meaning that both the emissions generated for electricity production and upstream emissions from fuel supply, such as fuel transport, are included in the transportation sector (Well-to-tank emissions) besides the sole activity-based emissions (Tank-to-wheel emissions).

The city uses traffic volume maps that represent the average weekday traffic on the major road network based on independent manual counts to calculate the activity. Minor roads are neglected. These volume maps are available for the total traffic and heavy goods traffic. Table 2 compares the annual VKT of the RKU with the numbers calculated in the present study for 2019. Multiple vehicle classes were aggregated to represent the same vehicle categories as the RKU uses. To extrapolate the weekday traffic volume to an annual traffic volume, the RKU multiplies the value by 365 days and a factor of 0.8 to account for reduced weekend traffic. In comparison, our results show a 5,2 % lower VKT for heavy goods traffic, a 7 % higher VKT for the remaining vehicle classes, and a 6.4 % higher total VKT. This is related to the different temporal scaling methods, including minor

https://doi.org/10.5194/egusphere-2025-753
Preprint. Discussion started: 10 April 2025

roads in the calculation (which account for approx. 11 % of the total VKT on an average weekday) and the different input data used.

Table 2. Comparison of the vehicle kilometers traveled (VKT) between the official greenhouse gas reporting of the City of Munich's Department for Climate and Environmental (RKU) and the calculations in the present study. Our calculation results in a 6.4 % higher VKT estimate than the RKU, which is caused by different temporal scaling methods and input data.

Vehicle Class	RKU [Mio. km]	DRIVE [Mio. km]	Difference
PC + LCV + MOT	5424,42	5836,74	+ 7,06 %
HGV + BUS	327,22	310,95	- 5,23 %
SUM	5751,64	6147,79	+ 6,44 %

3.2 Annual Emission Estimates

Table 3 shows the annual total emission estimates for 2019 to 2022 and the year-to-year change. The substantial decrease in all pollutants and GHGs in 2020 can be related to COVID-19, reduced traffic activity, and more fluid traffic, as shown above. Notably, air pollutants decrease by a higher share than CO_2. This change can be attributed to the ongoing development of emissions legislation, which improves the emissions performance of the entire fleet. The growing proportion of emission-free vehicles also contributes to this, although, despite the exponential increase in the electric vehicle share in 2020, they only account for about 1.8 % of the annual vehicle kilometers driven in Germany (Knörr et al., 2023).

On a national level, the total annual CO_2 emission of the road transport sector decreased by -12,6 % in 2020, by -0,7 % in 2021, and increased by 2,4 % in 2022. Total NO_x emissions decreased by -28,2 % in 2020, by -8,5 % in 2021, and by -5,5 % in 2022. For CO, the national authority reports a decrease of -23,7 % in 2020, a decrease of -3,2 % in 2021, and an increase of 4,3 % in 2022. (UBA, 2024) Similar trends are visible in the year-to-year change in Munich's annual emissions.

Table 3. Total traffic emission for CO_2 (fossil-fuel: $CO_{2,ff}$, fossil- and bio-fuel: $CO_{2,ff+bf}$), CO, NO_x, NO_2, PM and CH_4 in Munich. Total estimates and the year-to-year change from 2019 to 2022 are shown.

Component	Unit	2019		2020		2021		2022	
$CO_{2,ff}$	kt	1248,5	-	1050,1	-15,9%	1057,2	0,7%	1065,2	0,8%
$CO_{2,ff+bf}$	kt	1312,0	-	1121,2	-14,5%	1129,7	0,8%	1139,6	0,9%
CO	t	4194,0	-	3413,8	-18,6%	3303,2	-3,2%	3192,6	-3,3%
NO_x	t	3433,6	-	2581,5	-24,8%	2411,4	-6,6%	2148,4	-10,9%
NO_2	t	600,4	-	462,2	-23,0%	387,5	-16,2%	316,0	-18,5%
PM	t	44,8	-	35,6	-20,5%	31,9	-10,4%	30,0	-6%
CH_4	t	64,8	-	56,2	-13,3%	54,4	-3,2%	55,4	1,8%

https://doi.org/10.5194/egusphere-2025-753
Preprint. Discussion started: 10 April 2025

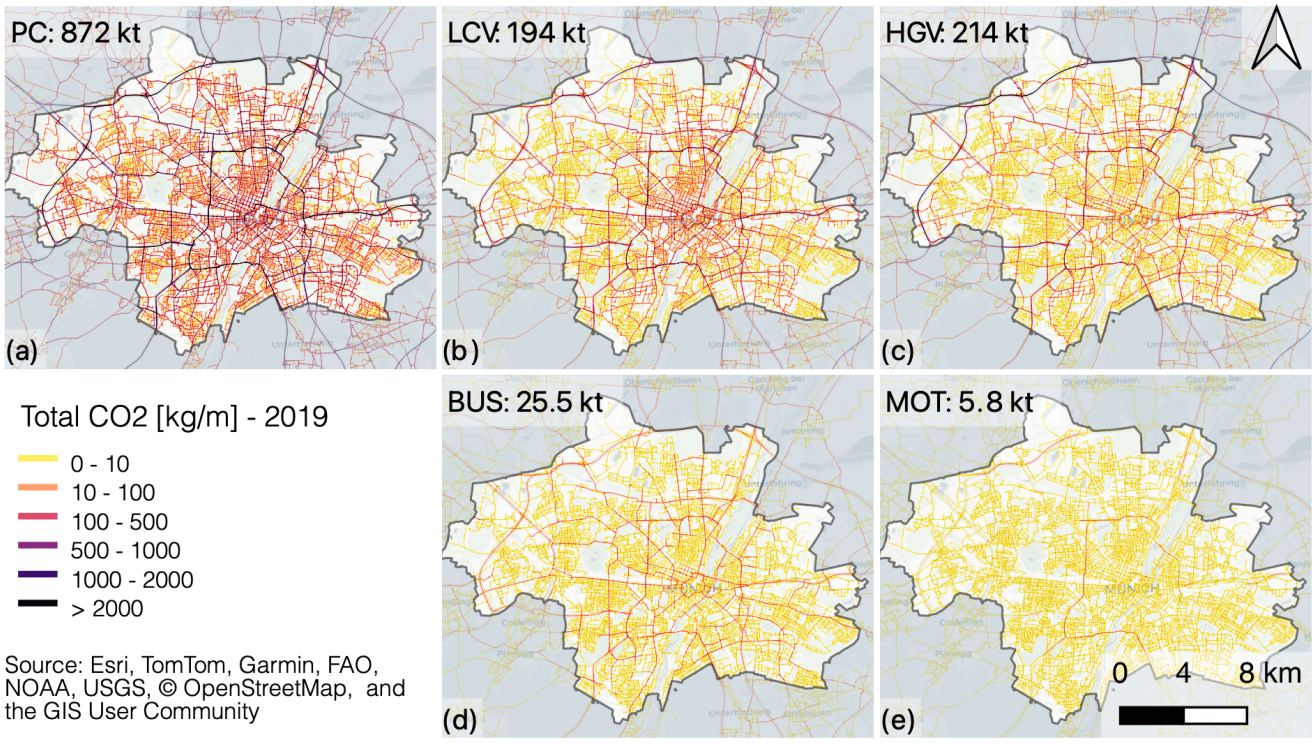

Figure 6. Spatial distribution of $CO_{2,ff+bf}$ emissions of different vehicle classes in 2019. Passenger cars (PC) account for the largest share in emissions. Followed by heavy goods vehicles and light commercial vehicles. High emission values on the main roads are visible for all vehicle classes. In total, buses and motorcycles only constitute 3% of Munich's emissions.

3.3 Spatial Distribution

Figure 6 depicts the spatial distribution of the emissions for different vehicle classes for 2019 as line sources along the road network. A dominant part (67 %) of the total CO_2 emissions comes from passenger car traffic, which can be seen in the color intensity of the upper left map (higher emissions are depicted with darker colors). Further, 30 % can be attributed to light commercial and heavy goods vehicle traffic. In total, buses and motorcycle emissions constitute 3 % of Munich's total CO_2 emissions. The spatial distributions are distinct and based on vehicle shares derived from the traffic model and the traffic counting data. The network of main roads is visible in the spatial distribution of the emissions.

In figure 7, we compare the spatial distribution of the total CO_2 emission with Germany's national inventory (referred to as UBA inventory) (Gniffke et al., 2024) and a European downscaled inventory (TNO GHGco v1.0) (Dellaert et al., 2019). Both use Germany's national estimates and disaggregate them with proprietary proxy maps. TNO utilizes open street map and open transport map-derived road networks and traffic volumes as well as population density. The UBA incorporates traffic volume as a proxy for the motorway and main roads. For further distribution to urban and rural roads, the UBA uses population density, number of registered vehicles per 1000 inhabitants, and spatial topology maps. Each inventory was gridded with a 1/60° latitude

https://doi.org/10.5194/egusphere-2025-753
Preprint. Discussion started: 10 April 2025

· 1/120° longitude (approximately 1 km · 1 km) grid, matching the original TNO grid's raster size and positioning. The cell values were normalized by the city total of each inventory to display them at a uniform scale.

The first row of the maps shows the spatial distribution of the individual inventories. TNO allocates a large share of emissions to the city center, where the population density is highest. While the layout of the main roads is visible, it is not particularly pronounced. The UBA inventory shows a more uniform distribution across the urban area, and the main roads are slightly more pronounced. The second row depicts difference maps between DRIVE, UBA, and TNO. Both downscaled inventories (UBA and TNO) attribute lower emissions to the main road network than DRIVE, with TNO attributing significantly higher emissions to the city center and UBA to urban residential areas. Based on local activity data, the DRIVE inventory assigns a substantial share of emissions to the main road network, accurately reflecting traffic volumes and congestion. In conclusion, proxies such as population density or spatial topology maps are not very representative of the spatial distribution of traffic emissions on a city scale. Local activity data is essential for distributing traffic emissions at the city level.

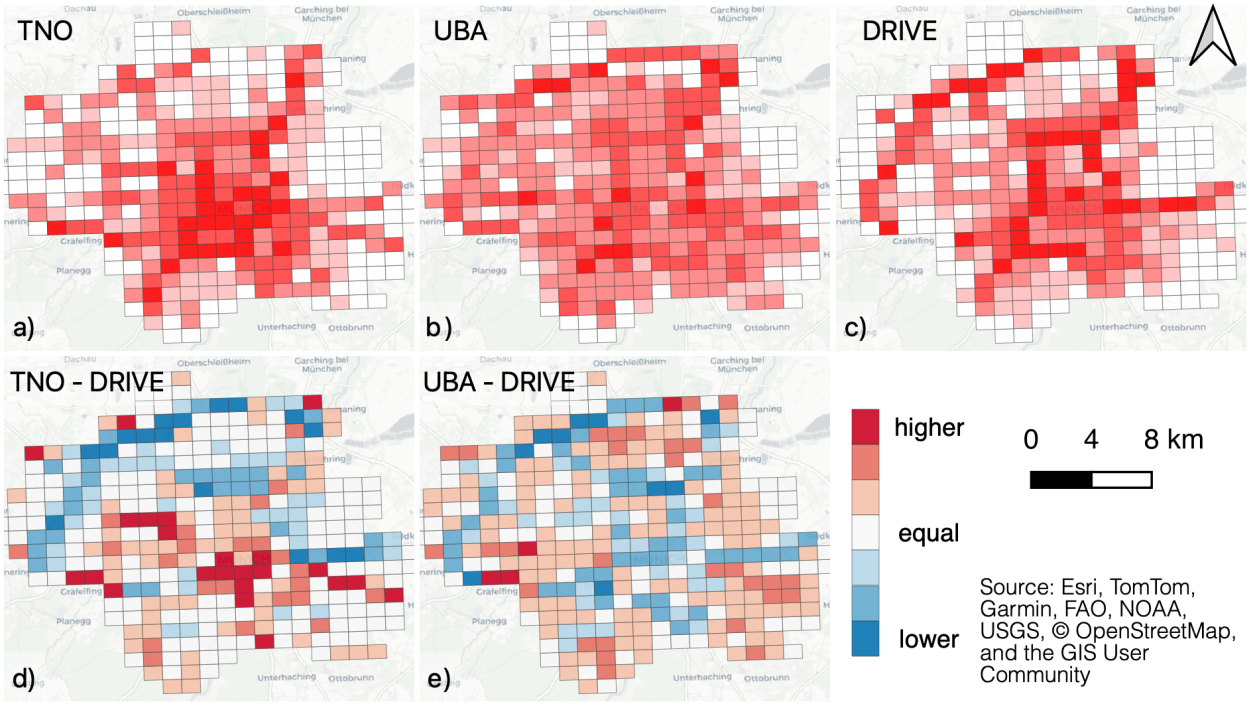

Figure 7. Comparison of the spatial distribution of CO_2 for the traffic sector from three inventory datasets. Plots (a)-(c) are standardized to the respective total values of the city to present them on a uniform scale. TNO (a) attributes major emissions to the city center, i.e., the place with the highest population density. The UBA shows a more homogeneous spatial distribution, and compared to the DRIVE inventory, roads with high traffic volumes are less pronounced. The difference plots in (d) and (e) indicate that UBA and TNO attribute lower emissions (blue) to the main road network and higher emissions (red) to minor roads. DRIVE uses validated local traffic activity data, more accurately representing the spatial distribution of related traffic emissions. Both downscaled inventories reflect the incorporated spatial proxies.

https://doi.org/10.5194/egusphere-2025-753
Preprint. Discussion started: 10 April 2025

Table 4 shows the emission totals for Munich and indicates large deviations between the datasets. The UBA attributes 47 % more while TNO attributes 24 % less CO_2 to the Munich region. The RKU reports 6.4 % less VKT but 6.2 % higher emissions, likely due to using a different emission factor database. For NO_x, the UBA shows 54 % higher values, while TNO indicates 14 % lower values. The $CO_{2,ff+bf}/NO_x$ ratios are very similar and range from 321 to 365, suggesting that the observed variations are due to differences in the underlying activity and proxy information rather than discrepancies in the emission factors.

For CO, the UBA attributes 287 % higher and TNO 83 % higher emissions. The $CO_{2,ff+bf}/CO$ ratio is 119 for UBA, 123 for TNO, and 297 for DRIVE and, therefore, cannot be attributed to different activity levels but emission factors. TNO and UBA distribute the same total emissions as reported by Germany. Consequently, the ratio between UBA and TNO falls within the same range. In our estimation, we noticed that CO emission factors in HBEFA are heavily dominated by petrol cars between Euro 4 and Euro 6ab. The emissions of these vehicles rise sharply at high speeds. Aggregated HBEFA emission factors are 5 times higher for the road category "motorway" and 2.5 times higher for "rural" compared to "urban". Accordingly, significant CO emissions are expected primarily on the motorway. The motorway accounts for approximately one-third of the total VKT in this study, and the traffic model indicates a maximum speed limit of 120 km/h for all motorway sections. In reality, however, the allowed speed is regulated depending on the traffic load, and often, no speed limit is applied. This indicates that we underestimate CO emissions at high free-flow speeds on the motorway (>130 km/h), while methods based on proxies overestimate the urban share. Both effects lead to significant deviations.

Table 4. Comparison of the total emission for fossil fuel CO_2 ($CO_{2,ff}$), fossil and biofuel CO_2 ($CO_{2,ff+bf}$), CO and NO_x from three different spatially explicit emission inventories in Munich (DRIVE, UBA, TNO). For this comparison, we selected the closest year available. The RKU estimate is the official number reported by the City of Munich and includes upstream emissions from the fuel supply chain (Scope 2). We compare the $CO_{2e,WTW}$ (Well-to-Wheel) emission in this case. All other emissions are tank-to-wheel, i.e., Scope 1 emissions.

Component	Unit	DRIVE (2019)	UBA (2019)		TNO (2018)		RKU (2019)	
$CO_{2,ff}$	kt	1248	-	-	946	- 24%		
$CO_{2,ff+bf}$	kt	1312	1936	+ 47%	993	- 24%		
CO	t	4194	16250	+ 287%	7671	+ 83%		
NO_x	t	3434	5299	+ 54%	2946	- 14%		
$CO_{2e,WTW}$	kt	1499	-	-	-	-	1592	+6.2 %
$CO_{2,ff+bf}/NO_x$		363,4	365,4		321,1		-	
$CO_{2,ff+bf}/CO$		297,6	119,1		123,3		-	

3.4 Temporal Profiles

Temporal profiles were calculated to distribute the annual emissions over time and to calculate the hourly emissions. These profiles contain scaling factors for the annual average hourly emissions, where the mean value of all scaling factors is 1. Different profiles were calculated for hot emissions and cold start excess emissions. The temporal distribution of cold start emissions

https://doi.org/10.5194/egusphere-2025-753
Preprint. Discussion started: 10 April 2025

is significantly influenced by the ambient temperature, which is also reflected by the profile. Additionally, the temporal profiles are strongly correlated with the traffic volume. The hot exhaust profile captures the non-linear relationship between traffic volume and emission factors. Increased traffic volume leads to congestion, resulting in higher emissions. Figure 8 depicts the temporal profile for hot exhaust and cold start excess emissions of different pollutants for 2019. In addition, it shows an example of a week in June 2019. The morning and afternoon peak hours are visible on working days. By contrast, a lower scaling factor, i.e., lower emissions, is assigned on weekends and holidays. The temporal profile for cold-start excess emissions shows a more irregular pattern as it strongly depends on the ambient temperature. The NO_x cold-start emission factor is negative for ambient temperatures above 25°C, which results in a negative scaling factor at the respective condition. This negative emission implies that NO_x emissions are lower during the cold start phase of the vehicle than when the vehicle exhaust system is hot.

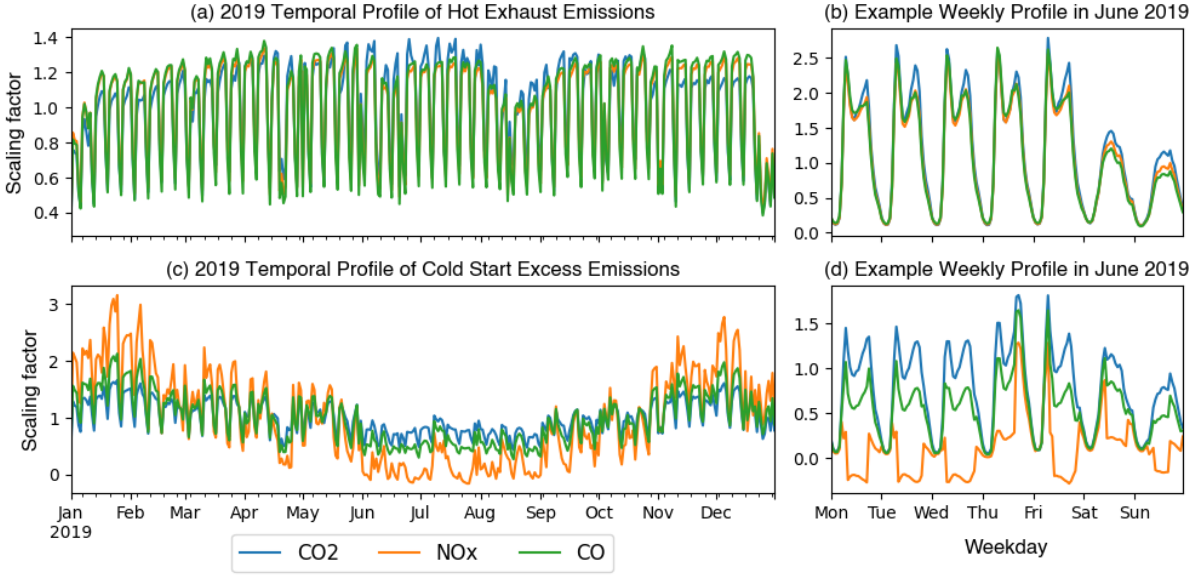

Figure 8. Temporal Scaling Factors for hot exhaust and cold-start excess emissions in 2019. Figure (a) illustrates the daily-averaged scaling factor for hot exhaust emissions, which closely follows traffic activity patterns. An example week in June 2019 (b) shows distinct rush-hour peaks during weekdays, while weekends generally have lower scaling factors due to reduced activity. Figures (c) and (d) illustrate the temporal profile of cold start excess emissions. Ambient temperature significantly affects this profile, leading to an annual cycle in the scaling factors. The discontinuities observed in the weekly cycle arise from the non-linear, value-binned emission factors for cold start excess emissions used in HBEFA.

https://doi.org/10.5194/egusphere-2025-753
Preprint. Discussion started: 10 April 2025

4 Uncertainty Analysis

4.1 Uncertainty of the Activity Data

The absolute uncertainty of the activity data ΔAD can be calculated by subtracting the modeled traffic volume from actual traffic counts measured by the traffic detector on the respective road link. Accordingly, the relative uncertainty $\frac{\Delta AD}{AD}$ is obtained by dividing the absolute error by the actual value, i.e., the counted traffic volume. This assessment was performed at an hourly, daily, and annual temporal aggregation, using the 2019 counting data from 64 counting stations. This traffic counting data is statistically independent as it was not used to calibrate the traffic model. Instead, the city uses manual counts and data from Germany's national mobility study MID (Mobilität in Deutschland (Nobis and Kuhnimhof, 2018)).

Figure 9 shows the analysis result. A systematic, positive bias can be observed for the hourly, daily, and annual traffic volume (Fig. 9 b, d, and f). The model slightly overestimates the traffic volume, especially at higher levels. However, it is also possible that the traffic counting stations, which are taken as the ground truth in this analysis, underestimate the volume of traffic, e.g. due to incorrect or missing counts or the malfunctioning of individual detectors. Lu et al. (2008) discusses loop fault detection and correction algorithms, but they require traffic data with higher temporal resolution than we use. In congested traffic situations, a combination of floating car data and traffic loop detector information shows superior performance in accurately estimating traffic variables compared to only using one data source (Qiu et al., 2010). Floating car data, however, is not available in our case. The counting data was assumed to be the ground truth to the best of our knowledge, and the effects mentioned were not examined in detail.

The 95 % confidence interval (95 % CI) of the relative deviation between detector and model values is (-48%, +109%) for hour values, (-34%, +66%) for daily values, and (-26%, +37%) for annual values. This shows a significant reduction in uncertainty with increasing temporal aggregation.

4.2 Uncertainty of the Emission Factor

Allekotte et al. (2023) examines the relative uncertainties of HBEFA emission factors $\frac{\Delta EF}{EF}$ for air pollutants nationally. The authors calculate uncertainties using Monte Carlo simulations. On average, a lower limit of -55 % to -10 % and an upper limit of +10 % to +90 % for regulated and non-regulated air pollutants was determined. However, the emission factors in the study are not based on the same granular activity rates as in HBEFA (*g/km*) but are expressed in *g/MJ* energy consumption. The emission factors were also aggregated according to different categories and distinguished between vehicle classes, pollutants, drive-train technologies, emission concepts, and road categories. Nevertheless, the uncertainties stated in this report were used because, to our current knowledge, this is the only information available on the uncertainty of HBEFA emission factors in Germany. Median upper and lower bounds for NO_x, CO, and $PM_{2.5}$ for the dominant vehicle categories PC, LCV, and HGV were extracted from the report. A weighted average was calculated based on the respective vehicle classes' total emissions. The report does not contain uncertainties for CO_2, as the calculation of CO_2 is based on energy source sales, and the approach for estimating its uncertainty is not model-based. On the national level, the 95 % CI for CO_2 ranges from $\pm 0.4\%$ for gasoline to $\pm 5\%$ for biodiesel. A conservative estimate of $\pm 5\%$ for all fuel and vehicle types is assumed. Table 5 shows the emission factor

https://doi.org/10.5194/egusphere-2025-753
Preprint. Discussion started: 10 April 2025

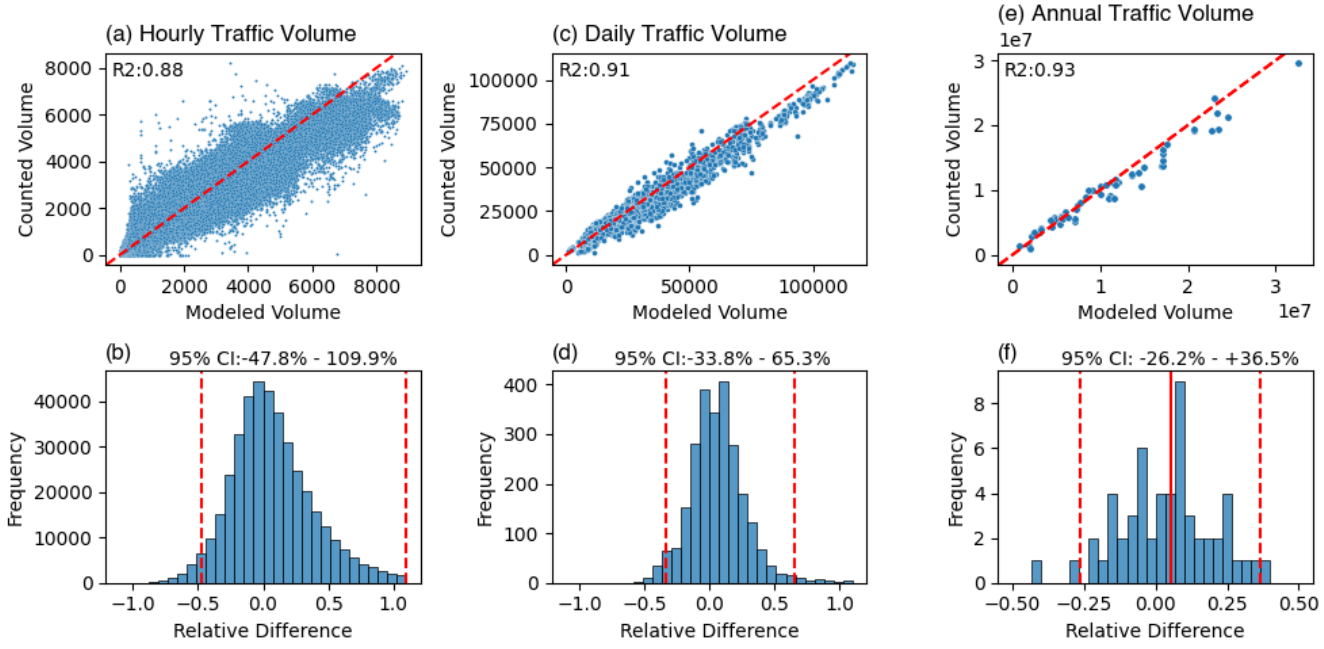

Figure 9. Uncertainty assessment of the activity data used in the present study: (a) and (b) show how hourly measured traffic counts match the modeled traffic volume for the total traffic in 64 detector locations in 2019. (c) and (d) illustrate the same for daily and (e,f) for annual traffic volumes. The model overestimates the traffic volume at higher levels. The 95 % confidence interval of the relative uncertainty significantly decreases with temporal aggregation, as expected. Considering the large extent of the traffic model and the high number of counting stations, these numbers can be well accepted.

uncertainties and distributions applied. Identical to Super et al. (2024), we assume a log-normal distribution and calculate the equivalent Gaussian standard deviation $\frac{\Delta EF}{EF}$ using equation 5.

$$\frac{\Delta EF}{EF} = \frac{ln(1+|lim_{upper}|) - ln(1-|lim_{lower}|)}{4} \tag{5}$$

Table 5. Emission factor uncertainties and distributions for air pollutants and carbon dioxide. The values were collected from the Allekotte et al. (2023) assessment of the uncertainties in HBEFA emission factors. The upper bound lim_{upper} and lower bound lim_{lower} were collected, and a $\frac{\Delta EF}{EF}$ for an equivalent Gaussian distribution was calculated.

Component	lim_{lower}	lim_{upper}	**Distribution**	$\frac{\Delta EF}{EF}$
NO_x	- 25 %	+ 31 %	log-normal	13.9 %
CO	- 33 %	+ 43 %	log-normal	19.0 %
$CO_{2,ff}$	- 5 %	+ 5 %	normal	2.5 %

https://doi.org/10.5194/egusphere-2025-753
Preprint. Discussion started: 10 April 2025

4.3 Uncertainty of the Emission Estimate

The traffic activity is used to estimate the traffic condition (see section 2.3), which is a fundamental parameter in selecting the emission factor. Therefore, traffic activity and the emission factor are correlated. This correlation, however, is not linear and cannot be determined analytically. We use the counted traffic volume and resulting volume-capacity ratio to calculate the emissions directly at the detector locations for methodological and computational simplicity. We then subtract the modeled emission of the respective road to calculate the absolute emission uncertainty ΔE^* and the relative uncertainty $\frac{\Delta E^*}{E^*}$ respectively. If the modeled and counted traffic volumes deviate so much from each other that different traffic conditions are estimated, this leads to significant variations in emissions. Therefore, the inclusion of data from multiple traffic counting stations introduces high variability to the estimated emissions. Emissions are overestimated in some areas and underestimated in others. Finally, the emission factor uncertainty $\frac{\Delta EF}{EF}$ is added to calculate the total emission uncertainty. The total emission uncertainty $\frac{\Delta E}{E}$ is approximated using equation 6.

$$\frac{\Delta E}{E} \approx \sqrt{\left(\frac{\Delta E^*}{E^*}\right)^2 + \left(\frac{\Delta EF}{EF}\right)^2} \tag{6}$$

The relative uncertainty of the emission estimate $\frac{\Delta E^*}{E^*}$, excluding the emission factor uncertainty, was calculated for hourly, daily, and annually aggregated emissions. A log-normal distribution with zero mean was fitted to the values within the 95% CI. Figure 10 shows the histogram and equivalent standard deviation of the relative emission uncertainty. We estimate 33.4% - 36.7% for hourly and 27.4 % - 27.8 % for daily values, depending on the pollutant. It shrinks from hourly to daily deviations for all three components. For annual aggregated values, the standard deviation increases to 26.0 % -29.4 % due to the greater significance of individual stations with strong deviations, i.e., systematic bias. If the detector value deviates significantly from the model value, then different traffic situations are estimated, which leads to a systematic deviation in the calculated emissions. Table 6 presents the total emission uncertainty $\frac{\Delta EF}{EF}$. The investigation focused on road links where traffic detectors were installed, ranging from short segments in densely interconnected urban areas to longer stretches on highways. We assume that emissions within 100 x 100 m grid cells exhibit identical levels of uncertainty due to a high spatial error correlation.

Table 6. Total Emission uncertainty $\frac{\Delta E}{E}$ at a road link level for CO_2, NO_x and CO. Three different values for different temporal aggregations are shown. Due to strong spatial error correlation, we assume identical uncertainty levels for emissions within 100 x 100 m grid cells.

Component	Hourly Uncertainty	Daily Uncertainty	Annual Uncertainty
NO_x	36,2 %	30.8 %	32,5 %
CO	41,3 %	33,7 %	32,2 %
$CO_{2,ff}$	33,9 %	27,5 %	28,5 %

https://doi.org/10.5194/egusphere-2025-753
Preprint. Discussion started: 10 April 2025

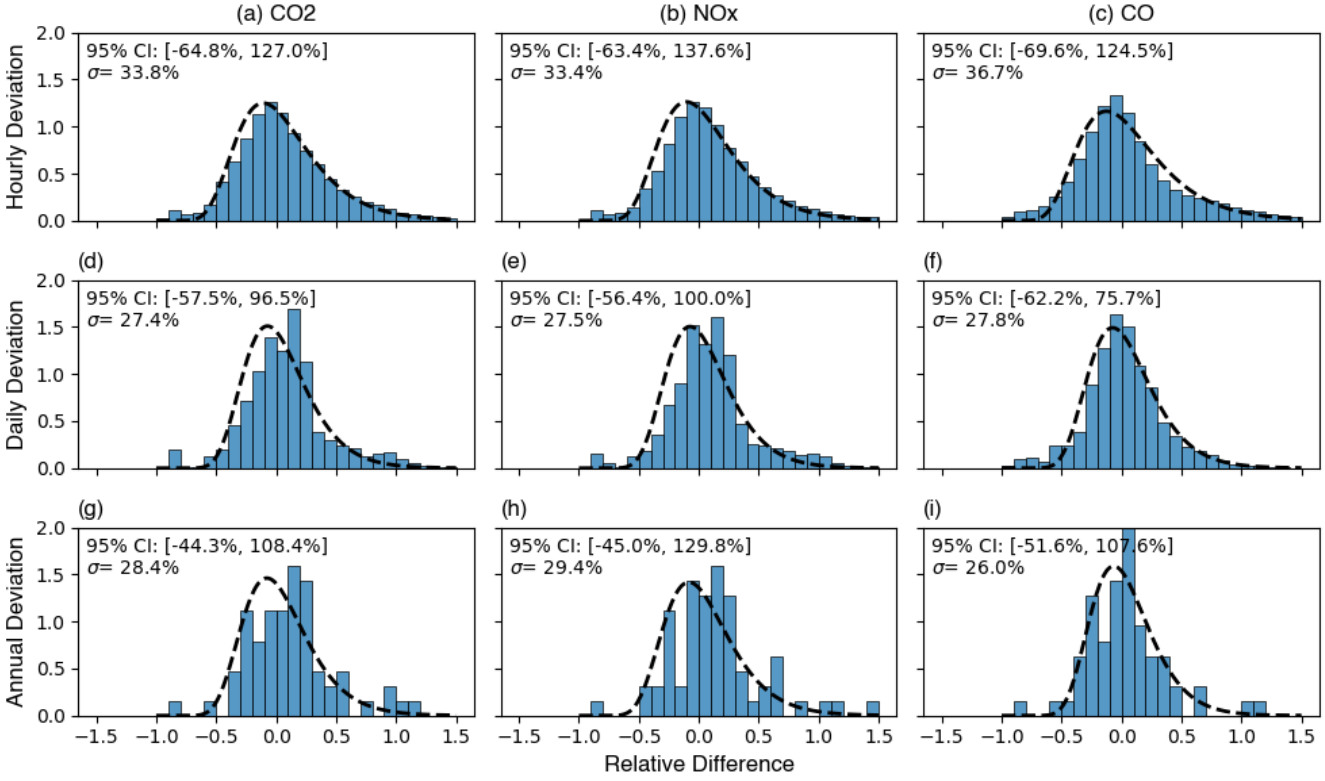

Figure 10. The estimated uncertainties $\frac{\Delta E^*}{E^*}$ for CO_2, NO_x, and CO emissions were calculated using traffic volumes and congestion levels from both modeled and counted data at 64 detector locations. The difference between model and detector emissions is shown for hourly (a-c), daily (d-f), and annual (g-i) aggregation levels. There is a noticeable reduction in relative uncertainty when moving from hourly to daily aggregation. However, when moving from daily to annual aggregation, the calculated values increase due to the higher significance of individual stations with strong deviations, resulting in less reliable statistics. A log-normal distribution with a zero mean is fitted to the data within the 95 % confidence interval, and the equivalent standard deviation was calculated.

4.4 Limitations of the Uncertainty Assessment

The uncertainty analysis focuses only on hot vehicle exhaust emissions and does not consider cold start emissions due to the lack of comparable data. This approach is adequate for CO_2 and NO_x, as these emissions are mainly generated when the engine is hot. For CO, strongly influenced by excess emissions during cold starts, the analysis likely underestimates the uncertainty because cold start emissions are more uncertain than hot emissions. Furthermore, on a city level, no specific information is available regarding the fleet composition, such as powertrain technologies and emission concepts, so statistical averages provided in HBEFA are used. These factors can vary significantly based on vehicle type, age, maintenance, and operating conditions, which may not be fully represented in a generalized dataset. Moreover, estimating traffic conditions using the volume capacity ratio is a simple, robust, and scalable method, yet it is not very accurate in urban road networks. The

https://doi.org/10.5194/egusphere-2025-753
Preprint. Discussion started: 10 April 2025

traffic flow is more often limited by the capacity of intersections than by the road links between them. The optimization applied (section 2.3) allows us to achieve a representative distribution of traffic conditions for the whole city on an annual average. However, we can not explicitly account for congestion effects such as queues and spillbacks. Despite these limitations, we assume the volume capacity ratio provides a reasonably accurate estimate of traffic conditions on the road link. But, at a road link level, congestion may introduce more uncertainty than reported. Finally, we do not explicitly take the correlation between traffic activity and the emission factor into account. If the traffic activity is estimated inaccurately, it leads to an incorrect traffic condition, and subsequently, a wrong emission factor is applied. A sensitivity analysis quantifying the impact of this correlation could further clarify its influence. The level of uncertainty also exhibits a daily pattern: at night, when traffic activity is low, the likelihood of a traffic jam is also low. However, during the day, especially during peak hours, the chances of experiencing traffic jams increase significantly. In future work, conducting a Monte Carlo simulation that incorporates the uncertainties related to traffic activity and emission factors during specific time periods could enable a probabilistic representation of how uncertainties propagate and better quantify the uncertainty of the emissions estimate.

5 Conclusions

We developed a road traffic emission inventory framework based on a macroscopic traffic model (static traffic model) and data from multiple traffic counting stations (dynamic traffic data). We utilize the counting data to extrapolate the traffic model temporally, increase the temporal resolution to one hour, and calculate hourly vehicle shares on different road types. The counted vehicle shares are then further adjusted using traffic model-based vehicle shares to account for spatial differences. In this way, we effectively combine the spatial information from the traffic model with the temporal information from the count data.

Based on the congestion level, road type, speed limit, road gradient, and vehicle class, the model selects the corresponding emission factor from the HBEFA 4.2 database. The congestion level is estimated using volume-capacity ratio thresholds optimized to reflect the national average distribution of traffic situations (Schmaus et al., 2023). By multiplying the emission factors by the vehicle-specific traffic volume and length of the road link, we achieve hourly hot exhaust emission estimates of different pollutants. To account for cold start excess emissions, the number of vehicle starts, which is included in the traffic model, was scaled using an average traffic activity profile. The hourly, local ambient temperature, averaged trip lengths, and parking durations were used to select emission factors for cold start emission calculations. Emission estimates are presented for 2019-2022.

In 2019, we estimate 6.2 % lower emissions compared to the city's assessment. However, we found significant differences compared to other spatially explicit, downscaled emission inventories. The German national inventory from UBA denotes 47 % higher, and TNO's European inventory 24 % lower CO_2 emissions to Munich. These proxy-based downscaling methods tend to underestimate traffic emissions along the leading road network and place a stronger emphasis on residential areas or places with high population density. This issue arises from the proxies used, which are not very representative of traffic

https://doi.org/10.5194/egusphere-2025-753
Preprint. Discussion started: 10 April 2025

emissions on an urban scale. Using local activity data and conducting a bottom-up estimation is essential to create an accurate emission map.

Finally, we assess the uncertainty of our estimates at a road-link-level resolution. The uncertainty arises from both the activity data and the emission factor. To assess the uncertainty in activity data, we compared the modeled traffic volume with actual counts from traffic counting stations. Our analysis demonstrates that uncertainty decreases as temporal aggregation increases. On an hourly basis, the 95 % confidence interval ($\pm 2\sigma$) is [-48 %, +109 %]; on a daily basis, it is [-34 %, +66 %]; and on an annual basis, it is [-25 %, +37 %]. Subsequently, we calculated the total emission uncertainty by estimating emissions using the counting data and comparing this estimate to the modeled emission of the respective road. The uncertainty, which we obtained from Allekotte et al. (2023), was added to this estimate. Total emission uncertainties (σ) range between 27.5 % to 41.3 % depending on the temporal aggregation level (hourly, daily, annual) and pollutant.

Emission inventories with high spatial and temporal resolution are fundamental for atmospheric modeling in urban areas. In particular, accurate temporal profiles are required to capture the temporal dynamics in high-resolution models, which is a limiting factor when using standard temporal profiles (Berchet et al., 2017). Our comprehensive use of counting data for vehicle class-specific temporal extrapolation has the potential to greatly improve the accuracy of atmospheric inversion in urban areas. The proposed framework effectively captures special events, such as COVID lockdowns, vacation periods, and individual holidays, and can also be adapted for near-real-time applications.

We see a lot of potential to further enhance the framework's capabilities by implementing methods to more accurately model the level and the location of congestion. While this is expected to change the result only modestly on the city scale, particular and localized emission hotspots are expected, which could inform policymakers where to target mitigation efforts (Tsanakas et al., 2020; Gately et al., 2017). Future work could include floating car data from TomTom or INRIX, providing actual vehicle speed information to more accurately model traffic congestion. Traffic congestion indexes, as used by Li et al. (2023), or microscopic traffic models that provide detailed movement information on individual vehicles, are another possible implementation in this regard.

Despite the limitations in accurately modeling traffic conditions and the limited knowledge of the local fleet composition, the proposed method provides a comprehensive, data-driven, and scalable approach to exploit static travel demand models and counting data from multiple traffic counting stations to estimate road transport emissions and their uncertainty. In future work, we will combine the transport inventory with high-resolution emissions data from other sectors such as heating, industry and public heat, power generation, and human respiration. This complete inventory can then be used in atmospheric modeling systems and optimized using the observations available in Munich.

Code and data availability. A code repository with detailed documentation and publicly available data sets is made available at https://doi.org/10.5281/zenodo.14644298 (Kühbacher et al., 2025). Updates and later versions can be accessed under https://github.com/tum-esm/drive-inventory

https://doi.org/10.5194/egusphere-2025-753
Preprint. Discussion started: 10 April 2025

Author contributions. DK designed and implemented the framework, performed all analysis, and wrote the original draft of the paper. JC provided supervision throughout the whole project. PA provided additional supervision at the early project phase. JC, PA, IS, and HDG provided methodological and scientific input and contributed to the analysis of the results at all stages of the project. MI provided scientific input on traffic engineering and contributed to the analysis of traffic-related results. The project was originally conceived by JC and HDG. All co-authors reviewed the manuscript and provided feedback.

Competing interests. The authors declare no competing interest.

Acknowledgements. We thank the City of Munich (Dr. Carlos Llorca Garcia, Verena Hartlieb and Wolfgang Qual) for data provision, insightful exchanges and general support of the topic. We also thank Stefan Feigenspan (Umweltbundesamt) for providing data and insights on Germany's national inventory. Further thanks go to Benedict Notter (INFRAS), who supported the comprehensive implementation of HBEFA, provided feedback on results and methodological suggestions. The authors also thank the IOCS Cities project and members who enabled the project. Finally, we thank Andreas Luther who reviewed the text.
For grammar and spell checking, DeepL and Grammarly were used.

Financial support. This work has been funded by the ICOS PAUL project: PAUL, Pilot Applications in Urban Landscapes - Towards integrated city observatories for greenhouse gases (ICOS Cities), funded by the European Union's Horizon 2020 Research and Innovation Programme under grant agreement No 101037319. Furthermore, the work is partly supported by the ERC consolidator grant CoSense4Climate (Grant 101089203).

https://doi.org/10.5194/egusphere-2025-753
Preprint. Discussion started: 10 April 2025

Appendix A: List of Symbols

$E^{hot}_{i,p,vc}$	Hot exhaust emission for pollutant p of vehicle class vc on the i-th road link. 10
$EF^{hot}_{p,vc,r,s,v,los}$	Parameterized emission factor for hot exhaust emission calculation [g/km]. 9, 10
$E^{cold}_{i,p,vc}$	Cold-start excess emission of pollutant p and vehicle class vc on the i-th road link. 10
$EF^{cold}_{p,vc,T}$	Parameterized emission factor for excess emission calculation [g/vehicle start]. 10
T	Ambient temperature [°C]. 10
p	Index for different pollutants (e.g. CO_2, NO_x). 10
d	Day type (weekday, Saturday, Sunday/Holiday). 6
vc	Vehicle class: PC, LCV, HGV, MOT, BUS. 10
i	Index for different road links. 4
s_i	Slope of the road [%]. 4, 10
L_i	Road length of the i-th road link [km]. 9, 10
C_i	Hourly vehicle capacity of the i-th road link [veh/h]. 4, 9
v_i	Allowed speed of the i-th road link [km/h]. 4, 10
r_i	Road type of the i-th road link. 4, 6, 10
$q^{model}_{i,vc}$	Modeled average annual weekday traffic flow of the i-th road link [veh/day]. 4, 6
$\delta^{model}_{i,HGV}$	Heavy goods vehicle (HGV) share of the i-th road link in the traffic model. 7
$\delta^{model}_{i,LCV}$	Light cargo vehicle (LCV) share of the i-th road link in the traffic model. 7
$q^{count,ref}_{i,vc}$	Counted average annual weekday traffic flow of the i-th road link, if and counting station is assigned [veh/day]. 6
$q_{i,vc}$	Vehicle-specific hourly traffic flow of the i-th road link [veh/h]. 6, 9, 10
α_r	Daily, road type specific scaling factor (annual cycle). 6
$\beta_{vc,d}$	Hourly, road type, and vehicle class specific scaling factor (diurnal cycle). 6
$\delta_{vc,r}$	Daily road-type and vehicle class specific share (vehicle share). 6, 7
$\kappa_{i,vc}$	Vehicle share correction factor to account for spatial differences in the vehicle share among a single road type. 6, 7, 8
x_i	Traffic volume to capacity ratio. 9
n_{vc}	Passenger car equivalent of the vehicle class vc. 9, 25
N_{vc}	Number of vehicle starts of the vehicle class vc. 10
$\delta^{count,ref}_{HGV,r}$	Heavy goods vehicle (HGV) share based on the 2019 average weekday counting data of the respective road type. 7
$\delta^{count,ref}_{LCV,r}$	Light cargo vehicle (LCV) share based on the 2019 average weekday counting data of the respective road type. 7
$\frac{\Delta AD}{AD}$	Relative uncertainty of the activity data. 17
$\frac{\Delta EF}{EF}$	Relative uncertainty of the emission factor. 17, 18, 19
$\frac{\Delta E^*}{E^*}$	Relative uncertainty of the emission estimate without emission factor uncertainty. 19, 20
$\frac{\Delta E}{E}$	Relative uncertainty of the emission estimate including the emission factor uncertainty. 19

https://doi.org/10.5194/egusphere-2025-753
Preprint. Discussion started: 10 April 2025

Appendix B: Counting Data Model and Model Parameters

Table B1. Data model for traffic counting data from different sources. Data following this structure can be processed by the modules implemented in the framework.

	Column	Data Type	Description
PK	*index*	int	Unique index for each row of the dataset
FK	*road_link_id*	int	Assigns the data row to a road link in the traffic model
	date	timestamp	Date of the counting information
	vehicle_class	str	Vehicle class of the counting information
	road_type	str	Road type of the corresponding road segment
	day_type	int	0: norm-weekday, 1: weekday, 2: Saturday, 3: Sunday/Holiday
	complete	bool	True if the timeseries of the station covers more than 80 % of all days in the total timeframe of interest.
	sqv	bool	True if the observed 2019 average norm-weekday count fits the traffic model with $SQV \geq 0.6$
	daily_value	int	Daily total count
	1 ... *24*	int	Hourly counting values

Table B2. Vehicle categories and Passenger Car Unit (PCU) scaling factors n_{vc}

8+1 vehicle class	**HBEFA vehicle class** vc	**PCU scaling factor** n_{vc}
Passenger Car	Passenger Car - PC	1
Passenger Car w. Trailer		
Motorcycles	Motorcycles - MOT	1
Light Truck	Light Commercial Vehicle - LCV	1
Truck	Heavy Goods Vehicles - HGV	2.5
Truck w. Trailer		
Truck w. Semi-Trailer		
Bus	Coach - BUS	1.75
Not Classified	-	-

https://doi.org/10.5194/egusphere-2025-753
Preprint. Discussion started: 10 April 2025

Appendix C: Diurnal Cycles of all Vehicle Classes

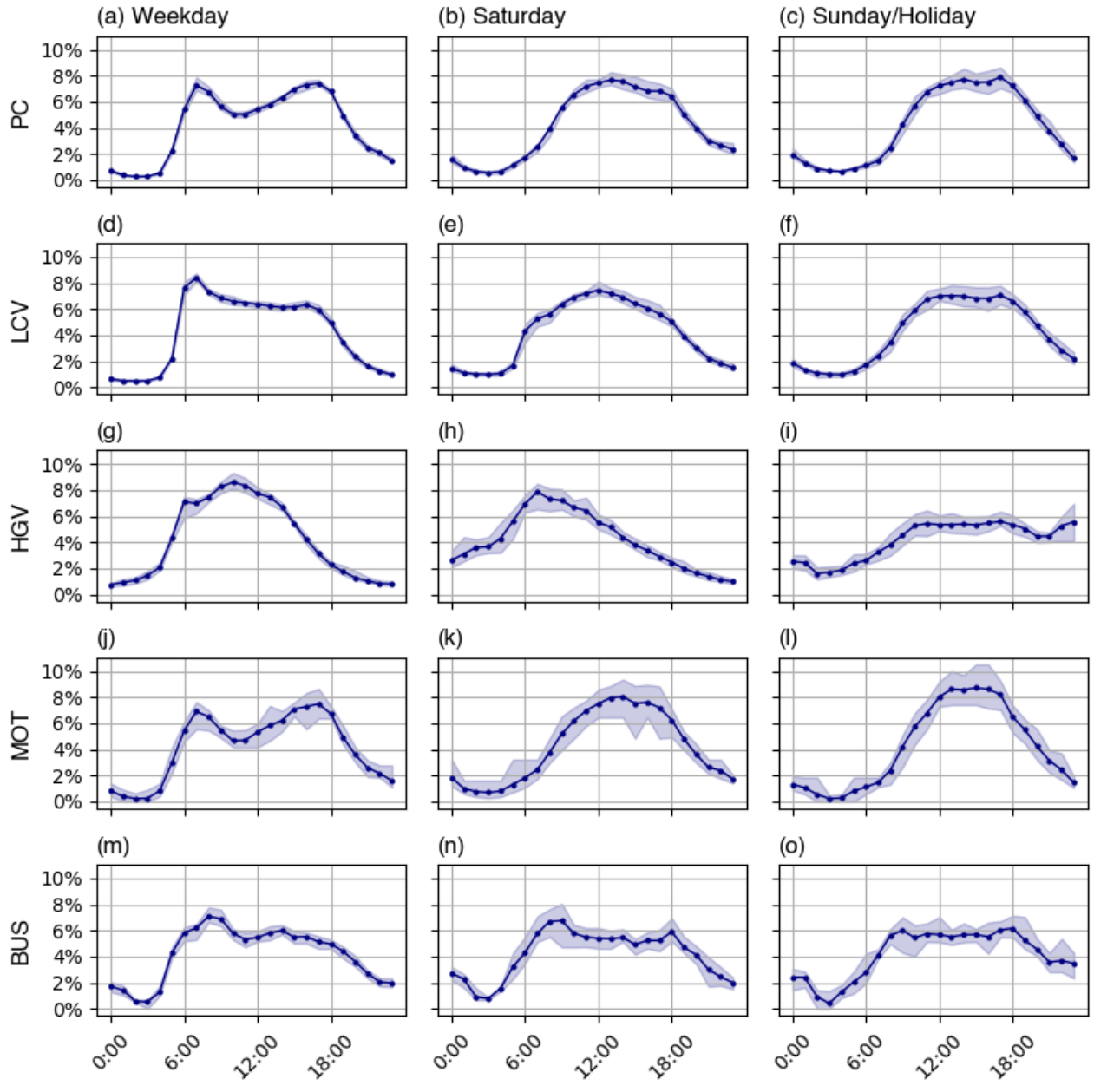

Figure C1. Individual cycles of all vehicle classes where emission factors are available in HBEFA. The blue line represents the average cycle for all months of the year, while the blue-shaded area indicates the range within which the cycles of individual months fall.

https://doi.org/10.5194/egusphere-2025-753
Preprint. Discussion started: 10 April 2025

References

WHO global air quality guidelines. Particulate matter (PM2.5 and PM10), ozone, nitrogen dioxide, sulfur dioxide and carbon monoxide., licence: CC BY-NC-SA 3.0 IGO, 2021.

Health Impacts of Air Pollution in Europe, 2022 — European Environment Agency, Web Report, European Environmental Agency (EEA), 2022.

Allekotte, M., Knörr, W., Kräck, J., Notter, B., Schäppi, B., Soini, M., Hausberger, S., Tödling, M., and Schadler, D.: Neubewertung der Unsicherheiten der mit den zur Berechnung der Luftschadstoffemissionen im Verkehrssektor verwendeten Parameter und Methoden, Tech. Rep. 152/2023, Umweltbundesamt, 2023.

Anke, J., Francke, A., Schaefer, L.-M., and Petzoldt, T.: Impact of SARS-CoV-2 on the Mobility Behaviour in Germany, European Transport Research Review, 13, 10, https://doi.org/10.1186/s12544-021-00469-3, 2021.

Arioli, M. S., D'Agosto, M. D. A., Amaral, F. G., and Cybis, H. B. B.: The Evolution of City-Scale GHG Emissions Inventory Methods: A Systematic Review, Environmental Impact Assessment Review, 80, 106 316, https://doi.org/10.1016/j.eiar.2019.106316, 2020.

Baek, B. H., Pedruzzi, R., Park, M., Wang, C.-T., Kim, Y., Song, C.-H., and Woo, J.-H.: The Comprehensive Automobile Research System (CARS) – a Python-based Automobile Emissions Inventory Model, Geoscientific Model Development, 15, 4757–4781, https://doi.org/10.5194/gmd-15-4757-2022, 2022.

Berchet, A., Zink, K., Oettl, D., Brunner, J., Emmenegger, L., and Brunner, D.: Evaluation of high-resolution GRAMM–GRAL (v15.12/v14.8) NOx simulations over the city of Zürich, Switzerland, 10, 3441–3459, https://doi.org/10.5194/gmd-10-3441-2017, 2017.

BMUB: Climate Action Plan 2050 – Principles and Goals of the German Government's Climate Policy, 2016.

Chan, E. C., Leitão, J., Kerschbaumer, A., and Butler, T. M.: Yeti 1.0: A Generalized Framework for Constructing Bottom-up Emission Inventories from Traffic Sources at Road-Link Resolutions, Geoscientific Model Development, 16, 1427–1444, https://doi.org/10.5194/gmd-16-1427-2023, 2023.

Chapman, L.: Transport and Climate Change: A Review, Journal of Transport Geography, 15, 354–367, https://doi.org/10.1016/j.jtrangeo.2006.11.008, 2007.

Creutzig, F., Lohrey, S., Emele, L., Le Quéré, C., and Jones, M.: COVID-19 und CO2-Emissionen in Deutschland: Eine Analyse basierend auf den Schätzungen des Global Carbon Projects.

Crippa, M., Guizzardi, D., Pisoni, E., Solazzo, E., Guion, A., Muntean, M., Florczyk, A., Schiavina, M., Melchiorri, M., and Hutfilter, A. F.: Global Anthropogenic Emissions in Urban Areas: Patterns, Trends, and Challenges, Environmental Research Letters, 16, 074 033, https://doi.org/10.1088/1748-9326/ac00e2, 2021.

Dellaert, S., Super, I., A., V., and van der Gon, H. D.: High Resolution Scenarios of CO2 and CO Emissions, https://www.che-project.eu/sites/default/files/2019-05/CHE-D4-2-V1-0.pdf, 2019.

EC-JRC: Including Cold-Start Emissions in the Real-Driving Emissions (RDE) Test Procedure: An Assessment of Cold Start Frequencies and Emission Effects., Publications Office, LU, 2017.

Edenhofer, O., R, P.-M., Y, S., E, F., S, K., K, S., A, A., I, B., S, B., P, E., B, K., J, S., S, S., C, v. S., T, Z., and J.C, M. e., eds.: Climate Change 2014: Mitigation of Climate Change: Working Group III Contribution to the Fifth Assessment Report of the Intergovernmental Panel on Climate Change, Cambridge University Press, New York, NY, ISBN 978-1-107-05821-7 978-1-107-65481-5, 2014.

https://doi.org/10.5194/egusphere-2025-753
Preprint. Discussion started: 10 April 2025

Friedrich, M., Pestel, E., Schiller, C., and Simon, R.: Scalable GEH: A Quality Measure for Comparing Observed and Modeled Single Values in a Travel Demand Model Validation, Transportation Research Record: Journal of the Transportation Research Board, 2673, 722–732, https://doi.org/10.1177/0361198119838849, 2019.

Gately, C. K., Hutyra, L. R., Peterson, S., and Wing, I. S.: Urban Emissions Hotspots: Quantifying Vehicle Congestion and Air Pollution Using Mobile Phone GPS Data, Environmental Pollution, 229, 496–504, https://doi.org/10.1016/j.envpol.2017.05.091, 2017.

Gniffke, P., Kotzulla, M., and Hausmann, K.: German Informative Inventory Report 2024, Web Report, Umweltbundesamt (UBA), Berlin, 2024.

Guevara, M., Jorba, O., Tena, C., Denier van der Gon, H., Kuenen, J., Elguindi, N., Darras, S., Granier, C., and Pérez García-Pando, C.: Copernicus Atmosphere Monitoring Service TEMPOral Profiles (CAMS-TEMPO): Global and European Emission Temporal Profile Maps for Atmospheric Chemistry Modelling, Earth System Science Data, 13, 367–404, https://doi.org/10.5194/essd-13-367-2021, 2021.

Hausberger, S.: Simulation of Real World Vehicle Exhaust Emissions, vol. 82, KM-THD Mitteilungen Technical University Graz, 2003.

Hutchins, M. G., Colby, J. D., Marland, G., and Marland, E.: A Comparison of Five High-Resolution Spatially-Explicit, Fossil-Fuel, Carbon Dioxide Emission Inventories for the United States, Mitigation and Adaptation Strategies for Global Change, 22, 947–972, https://doi.org/10.1007/s11027-016-9709-9, 2017.

Ibarra-Espinosa, S., Ynoue, R., O'Sullivan, S., Pebesma, E., Andrade, M. D. F., and Osses, M.: VEIN v0.2.2: An R Package for Bottom–up Vehicular Emissions Inventories, Geoscientific Model Development, 11, 2209–2229, https://doi.org/10.5194/gmd-11-2209-2018, 2018.

IEA: Empowering Urban Energy Transitions, https://www.iea.org/reports/empowering-urban-energy-transitions, 2024.

IFEU: Methodenpapier Kurzfassung: Bilanzierungssystematik kommunaler Treibhausgasemissionen (BISKO), Tech. rep., Institut für Energie- und Umweltforschung Heidelberg GmbH (ifeu), https://www.ifeu.de/fileadmin/uploads/BISKO_Methodenpapier_kurz_ifeu_Nov19.pdf, accessed: 2024-10-30, 2019.

Iglewicz Boris and David C. Hoaglin: How to Detect and Handle Outliers, vol. 16, American Society for Quality Control - Statistics Devision, ISBN 0-87389-247-X, 1993.

Jiang, L., Xia, Y., Wang, L., Chen, X., Ye, J., Hou, T., Wang, L., Zhang, Y., Li, M., Li, Z., Song, Z., Jiang, Y., Liu, W., Li, P., Rosenfeld, D., Seinfeld, J. H., and Yu, S.: Hyperfine-Resolution Mapping of on-Road Vehicle Emissions with Comprehensive Traffic Monitoring and an Intelligent Transportation System, Atmospheric Chemistry and Physics, 21, 16 985–17 002, https://doi.org/10.5194/acp-21-16985-2021, 2021.

Knörr, W., Heidt, C., Gores, S., and Bergk, F.: Fortschreibung des Daten- und Rechenmodells: Energieverbrauch und Schadstoffemissionen des motorisierten Verkehrs in Deutschland 1960-2035, sowie TREMOD, im Auftrag des Umweltbundesamtes, Tech. rep., Ifeu Institut für Energie- und Umweltforschung Heidelberg GmbH, Heidelberg & Berlin, 2023.

Kuenen, J., Dellaert, S., Visschedijk, A., Jalkanen, J.-P., Super, I., and Denier van der Gon, H.: CAMS-REG-v4: A State-of-the-Art High-Resolution European Emission Inventory for Air Quality Modelling, Earth System Science Data, 14, 491–515, https://doi.org/10.5194/essd-14-491-2022, 2022.

Kühbacher, D., Chen, J., Aigner, P., Denier van der Gon, H., Super, I., and Ilic, M.: DRIVE v1.0 - A data-driven framework to estimate road transport emissions and temporal profiles (v1.0), https://doi.org/10.5281/zenodo.14644298, 2025.

Li, X., Gu, D., Hohenberger, T. L., Fung, Y. H., Fung, J. C., Lau, A. K., and Liang, Z.: Dynamic quantification of on-road emissions in Hong Kong: Impact from traffic congestion and fleet composition variation, 313, 120 059, https://doi.org/10.1016/j.atmosenv.2023.120059, 2023.

https://doi.org/10.5194/egusphere-2025-753
Preprint. Discussion started: 10 April 2025

Lu, X.-Y., P. Varaiya, R. Horowitz, and J. Palen: Faulty Loop Data Analysis and Loop Fault Detection, in: 15th ITS World Congress, Unpublished, https://doi.org/10.13140/2.1.2654.0802, 2008.

Nobis, C. and Kuhnimhof, T.: Mobilität in Deutschland – MiD Ergebnisbericht. Studie von infas, DLR, IVT und infas 360 im Auftrag des Bundesministers für Verkehr und digitale Infrastruktur (FE-Nr. 70.904/15), www.mobilitaet-in-deutschland.de, 2018.

Notter, B., Keller, M., Althaus, H.-J., Cox, B., Knörr, W., Heidt, C., Biemann, K., Räder, D., and Jamet, M.: HBEFA 4.1 Development Report, 2019.

Ntziachristos, L. and Samaras, Z.: EMEP/EEA air pollutant emission inventory guidebook 2023 – Update 2024, https://copert.emisia.com/wp-content/uploads/2024/07/1.A.3.b.i-iv-Road-transport-2024.pdf, 2024.

Oda, T. and Maksyutov, S.: A Very High-Resolution (1 Km×1 Km) Global Fossil Fuel CO_2 Emission Inventory Derived Using a Point Source Database and Satellite Observations of Nighttime Lights, Atmospheric Chemistry and Physics, 11, 543–556, https://doi.org/10.5194/acp-11-543-2011, 2011.

Oda, T., Maksyutov, S., and Andres, R. J.: The Open-source Data Inventory for Anthropogenic CO_2, version 2016 (ODIAC2016): a global monthly fossil fuel CO_2 gridded emissions data product for tracer transport simulations and surface flux inversions, Earth System Science Data, 10, 87–107, https://doi.org/10.5194/essd-10-87-2018, 2018.

Pinto, J. A., Kumar, P., Alonso, M. F., Andreao, W. L., Pedruzzi, R., dos Santos, F. S., Moreira, D. M., and de Almeida Albuquerque, T. T.: Traffic Data in Air Quality Modeling: A Review of Key Variables, Improvements in Results, Open Problems and Challenges in Current Research, Atmospheric Pollution Research, 11, 454–468, https://doi.org/10.1016/j.apr.2019.11.018, 2020.

Qiu, T. Z., Lu, X.-Y., Chow, A. H. F., and Shladover, S. E.: Estimation of Freeway Traffic Density with Loop Detector and Probe Vehicle Data, Transportation Research Record, 2178, 21–29, https://doi.org/10.3141/2178-03, 2010.

Referat für Klima und Umweltschutz: Treibhausgas-Monitoring der Landeshauptstadt München 1990 bis 2019; Sitzungsvorlage 20-26 / V 06797, https://risi.muenchen.de/risi/sitzungsvorlage/detail/7205164, 2022.

Rodriguez-Rey, D., Guevara, M., Linares, M. P., Casanovas, J., Salmerón, J., Soret, A., Jorba, O., Tena, C., and Pérez García-Pando, C.: A Coupled Macroscopic Traffic and Pollutant Emission Modelling System for Barcelona, Transportation Research Part D: Transport and Environment, 92, 102 725, https://doi.org/10.1016/j.trd.2021.102725, 2021.

Schmaus, M., Bawidamann, J., Friedrich, M., Haberl, M., Trenkwalder, L., Fellendorf, M., Uhlig, J., Lohse, R., and Pestel, E.: Flüssiger Verkehr für Klimaschutz und Luftreinhaltung, Final report 14/2023, Umweltbundesamt (UBA), 2023.

Schneider, C., Pelzer, M., Toenges-Schuller, N., Nacken, M., and Niederau, A.: ArcGIS basierte Lösung zur detaillierten, deutsch-landweiten Verteilung (Gridding) nationaler Emissionsjahreswerte auf Basis des Inventars zur Emissionsberichterstattung, Tech. rep., Umweltbundesamt, 2016.

Smit, R., Ntziachristos, L., and Boulter, P.: Validation of Road Vehicle and Traffic Emission Models A Review and Meta-Analysis, Atmospheric Environment, 44, 2943–2953, https://doi.org/10.1016/j.atmosenv.2010.05.022, 2010.

Super, I., Dellaert, S. N. C., Visschedijk, A. J. H., and van der Gon, H. A. C. D.: Uncertainty Analysis of a European High-Resolution Emission Inventory of CO2 and CO to Support Inverse Modelling and Network Design, Atmospheric Chemistry and Physics, 20, 1795–1816, https://doi.org/10.5194/acp-20-1795-2020, 2020.

Super, I., Scarpelli, T., Droste, A., and Palmer, P. I.: Improved definition of prior uncertainties in CO_2 and CO fossil fuel fluxes and the impact on a multi-species inversion with GEOS-Chem (v12.5), EGUsphere, 2024, 1–34, https://doi.org/10.5194/egusphere-2023-2025, 2024.

https://doi.org/10.5194/egusphere-2025-753
Preprint. Discussion started: 10 April 2025

Timpe, C., Kenkmann, T., Hesse, T., Mundt, J., Maaß, C., Kapfer, J., Claas-Reuther, J., Rudolf, A., and Kluth, T.: Maßnahmenplan Klimaneutralität München, https://stadt.muenchen.de/dam/jcr:dc76020e-b14b-42ca-9eea-4c3ce538b951/Massnahmenplan-Klimaneutralitaet-Muenchen.pdf, 2021.

Ting Wei, Junliang Wu, and Shaoqing Chen: Keeping Track of Greenhouse Gas Emission Reduction Progress and Targets in 167 Cities Worldwide, 2021.

Tsanakas, N., Ekström, J., and Olstam, J.: Estimating Emissions from Static Traffic Models: Problems and Solutions, pp. 1–17, https://doi.org/10.1155/2020/5401792, 2020.

UBA: Submission under the United Nations Framework Convention on Climate Change 2024, 2024.

Wen, Y., Zhang, S., Zhang, J., Bao, S., Wu, X., Yang, D., and Wu, Y.: Mapping Dynamic Road Emissions for a Megacity by Using Open-Access Traffic Congestion Index Data, Applied Energy, 260, 114 357–114 357, https://doi.org/10.1016/j.apenergy.2019.114357, 2020.

Wu, L., Chang, M., Wang, X., Hang, J., Zhang, J., Wu, L., and Shao, M.: Development of the Real-time On-road Emission (ROE v1.0) Model for Street-Scale Air Quality Modeling Based on Dynamic Traffic Big Data, Geoscientific Model Development, 13, 23–40, https://doi.org/10.5194/gmd-13-23-2020, 2020.

Yang, D., Zhang, S., Niu, T., Wang, Y., Xu, H., Zhang, K. M., and Wu, Y.: High-Resolution Mapping of Vehicle Emissions of Atmospheric Pollutants Based on Large-Scale, Real-World Traffic Datasets, Atmospheric Chemistry and Physics, 19, 8831–8843, https://doi.org/10.5194/acp-19-8831-2019, 2019.